

# THE PS BOOSTER ALIGNMENT CAMPAIGN AND A NEW TUNE CONTROL IMPLEMENTATION AFTER THE LHC INJECTORS UPGRADE AT CERN

F. Antoniou\*, F. Asvesta, H. Bartosik, J-F. Comblin, G. P. Di Giovanni, M. Hostettler, A. Huschauer, B. Mikulec, J. M. Nonglaton, T. Prebibaj<sup>1</sup>, CERN, Geneva, Switzerland  
<sup>1</sup>also at Goethe University, Frankfurt, Germany

## Abstract

The CERN PS Booster (PSB) has gone through major upgrades during the Long Shutdown 2 (LS2) and the recommissioning with beam started in December 2020. Two of the aspects leading to improved operation will be described in this paper: a new tune control implementation; and a full re-alignment campaign. The operation of the PSB requires a large range of working points to be accessible, with a dynamic change of tunes along the acceleration cycle. Before LS2, the PSB tune control was based on an analytical approach assuming linear magnet transfer functions. As part of the LIU project, the PSB main power supply was upgraded to raise the extraction energy from 1.4 GeV to 2 GeV, in order to improve the brightness reach of the downstream machines. A new tune control implementation was necessary to take into account saturation effects of the bending magnets and the reconfiguration of the main circuits, as well as the additional complexity of the new H<sup>-</sup> charge exchange injection. The first part of the paper describes the implementation of the new tune control and its experimental verification and optimization. The second part describes the results of the PSB alignment campaign after LS2, giving emphasis to the method developed to perform a combined closed orbit correction through quadrupole alignments.

## THE NEW PSB TUNE CONTROL

The operation of the PSB requires a large range of working points to be accessible, with a dynamic change of tunes along the acceleration cycle. Pre-LS2, the tune control implementation in the PSB was based on an analytical approach, which assumed linear magnet transfer functions [1]. This approach was proven to give a good agreement between the programmed and the measured machine tune with maximum discrepancies between the two of about  $\Delta Q \approx 0.01$ .

After LS2, the production of the high brightness LHC beams required a raise in the the PSB extraction energy from 1.4 GeV to 2 GeV in order to mitigate space charge effects in the PS. Therefore, the main power supply of the PSB was upgraded as part of the LIU project. Due to the higher operation energies, the main bending magnets of the PSB now operate in their saturation regime. To take into account the increased complexity due to the reconfiguration of the main circuits and the saturation effects of the bending magnets, as well as the additional impact of the new H<sup>-</sup> charge exchange injection [2], a new tune control scheme

was implemented during LS2. This new implementation consists of three main modules:

1. The Q-editor application to set the tune functions along the cycle for each of the four rings of the PSB individually.
2. A make rule “Q → K” for determining the required quadrupole strengths (K) based on the requested tunes (Q). This is using the analytical description of the PSB lattice already employed pre-LS2.
3. A make rule for the translation from the required quadrupole strengths (K) to the respective power supply current (I), as well as the sharing of the power supply current among the different current circuits. This requires as input the calibration curves for the various magnets, taking into account the saturation at high currents and the differences between the magnet transfer functions for inner and outer rings.

## The PSB Main Magnet Circuits

The configuration of the main magnet circuits of the PSB after LS2 is shown in Fig. 1 [3, 4]. It consists of:

- Two dipole circuits: one circuit common for all the bending magnets of the external rings (BR14) and all the 128 QFO focusing quadrupoles for all four rings. The current in this circuit will be denoted as  $I_{b,ext}$ . The other dipole circuit is common for all the bending magnets of the internal rings (BR23) and all the 64 QDE

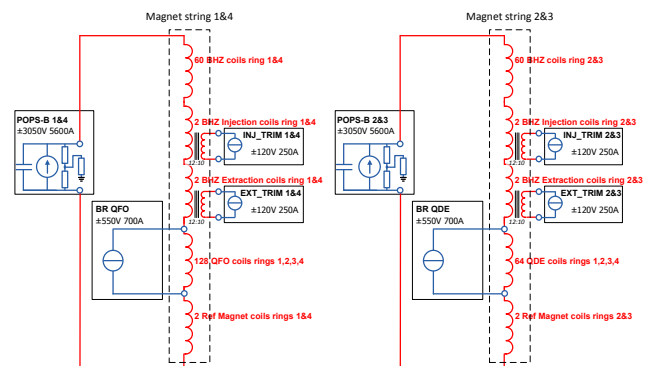


Figure 1: Main PSB power converter circuits after the LIU upgrade [3, 4].

\* fanouria.antoniou@cern.ch

defocusing quadrupoles for all four rings, with the corresponding current denoted as  $I_{b,int}$ .

- Additional trim power converters for the dipoles in the injection and extraction regions to compensate for differences in the calibration curves of these special magnets, that may arise from the modified yoke required for injection/extraction. These trims are individual for each of these magnets and for inner and outer rings.
- Trim power supplies for the QFO and QDE magnets, common for all the four rings, used for the base tune control. The current going through the QFO trim converters will be denoted as  $I_f$ , while the one going through the QDE trim converters as  $I_d$ .
- Q-strip circuits on the focusing (QCF circuit) and defocusing quadrupoles (QCD circuits) with separate circuits for each ring, which can be used for ring-by-ring tune adjustments. The current going through these circuits will be denoted as  $\Delta I_f$  and  $\Delta I_d$ , respectively.
- For the compensation of the beta-beat induced by the injection chicane, there will be two additional fast power supplies for the Q-strips on magnets QDE3 and QDE14 per ring to allow for optics corrections for each ring individually. The Q-strip windings on these magnets are not part of the main Q-strip circuits (QCF and QCD).

### Calibration Curves from Magnetic Measurements

With the new extraction energy in the PSB (2 GeV), the main bending magnets now operate in their saturation regime. As the bending magnets share a common circuit with the quadrupoles, the calibration curves are an important input for the tune control implementation.

During LS2, detailed magnetic measurements were performed for the PSB main bending magnets and the special injection and extraction magnets [5–7]. The following fit function was applied to the measured data for defining the calibration curves of the three types of main magnets for all rings, as proposed in [8]:

$$Bdl = Bdl_{rem} + kI_b \left( 1 - \left( \frac{I_b}{I_0} \right)^n \right), \quad (1)$$

where  $Bdl_{rem}$  is the remnant field at zero current and  $I_b$  the current going through the bending magnets. The parameters  $k$ ,  $I_0$  and  $n$  are defined through a fitting routine. The remnant field is based on magnetic measurements [9].

Figure 2 shows the difference between the measured and fitted integrated field as a function of the excitation current for the main dipoles of Ring 1 (top) and Ring 2 (bottom). The results corresponding to a linear fit are shown in blue, while the ones corresponding to the non-linear fit (Eq. (1)) in orange. The deviation from the linear fit at high currents is due to the saturation of the magnets, which is more pronounced for the external (1 and 4) than the internal (2 and 3) rings. This observation is similar for all rings and for the different types of bending magnets. The fit coefficients of

Eq. (1) are summarized in Table 1 for all types of bending magnets.

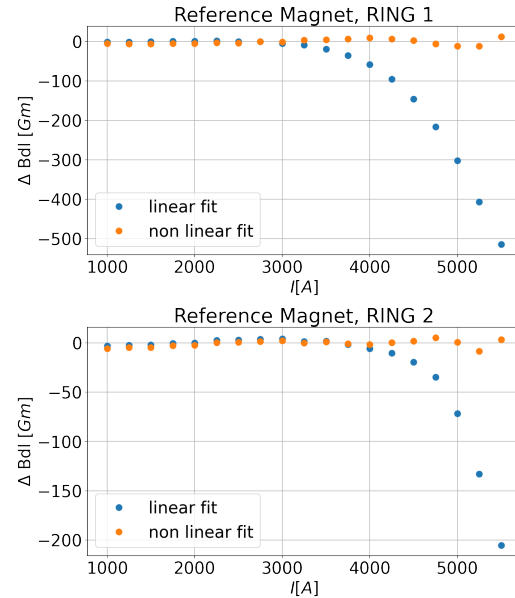


Figure 2: Difference between measured and fitted integrated field as a function of excitation current for the main bending magnets of Ring 1 (top) and Ring 2 (bottom).

Table 1: Fit Coefficients for the Calibration Curves of the PSB Bending Magnets

| Dipole type         | $I_0$     | $k$       | $n$     |
|---------------------|-----------|-----------|---------|
| Main (BR23)         | 8.4911e+3 | 3.4817e-4 | 10.3555 |
| Main (BR14)         | 1.0609e+4 | 3.4870e-4 | 5.4973  |
| Special inj. (BR23) | 1.6855e+4 | 3.4824e-4 | 5.3194  |
| Special inj. (BR14) | 1.0014e+4 | 3.4800e-4 | 6.1358  |
| Special ext. (BR23) | 1.4347e+4 | 3.4817e-4 | 5.9844  |
| Special ext. (BR14) | 1.0031e+4 | 3.4815e-4 | 6.1280  |

Magnetic measurements were also performed for the focusing (QFO) and defocusing (QDE) quadrupole magnets. A linear fit of the data was applied, as the quadrupoles still operate in their linear regime up to the new extraction energy of 2 GeV.

In the new tune control implementation, the measured calibration curves are taken into account both for the main bending and the quadrupole magnets. The quadrupole strengths as a function of the power supply currents can be written in the more general form:

$$K_{f,i} = \frac{C_{f,i}/L_f}{B\rho} \times (I_{b,ext} + I_f + 0.5 \cdot \Delta I_{f,i}), \quad (2)$$

$$K_{d,i} = \frac{C_{d,i}/L_d}{B\rho} \times (I_{b,int} + I_d + 0.5 \cdot \Delta I_{d,i}),$$

where the index  $i$  refers to the ring number.  $I_{b,int}$  and  $I_{b,ext}$  are the currents in the main circuits passing from the internal ( $i = 2, 3$ ) and external ( $i = 1, 4$ ) rings respectively.  $C_{f,i}$  and  $C_{d,i}$  are the calibration factors of the focusing and

defocusing quadrupoles.  $I_f$  and  $I_d$  are the currents in the trim power supply circuits going through the focusing and defocusing quadrupoles respectively, and they are common for all rings. The factor 0.5 for the currents of the Q-strip power converters  $\Delta I_{f,d}$  is due to the fact that the main coils of the quadrupoles have twice the number of turns compared to the trim coils of the Q-strip circuits. The total current needed from the quadrupole power supplies for achieving the required strengths is obtained by inversion of Eq. (2).

To increase the tuning range in case different tune functions are programmed for each ring, the currents in the QFO and QDE trim power supply circuits common to all rings are chosen as:

$$\begin{aligned} I_f &= \left( \min(I_{f,i})_{i=1-4} + \max(I_{f,i})_{i=1-4} \right) / 2, \\ I_d &= \left( \min(I_{d,i})_{i=1-4} + \max(I_{d,i})_{i=1-4} \right) / 2, \end{aligned} \quad (3)$$

where the max and min is computed among all the rings. The currents  $I_f$  and  $I_d$  will be clamped to the maximum available from the corresponding quadrupole trim power converters.

In the case that ring-by-ring tune adjustments are needed, i.e. if the tune functions per ring are not all the same, the currents in the Q-strips ( $\Delta I_{d,i}$  and  $\Delta I_{f,i}$ ) are used to provide the extra correction on the focusing or defocusing strengths ( $\Delta K_{f,i}$  and  $\Delta K_{d,i}$ ), based again on inversion of Eq. (2).

### Commissioning of the New PSB Tune Control

The new PSB tune control implementation was tested already in the first part of the beam commissioning period. The first checks for the validation of the implementation were done by applying relative tune changes through the tune control application. The measured tune followed the relative changes very well, demonstrating that the new tune control was correctly implemented.

Comparing the absolute values of the set and measured tunes though, showed an increased difference between these values, as well as tune oscillations along the cycle. This initial tune difference as a function of the cycle time is shown in blue in Fig. 3, for R1 (left) and R2 (right). The behavior of R3 and R4 is similar to the ones of R2 and R1 respectively. The observed tune oscillations along the cycle are well correlated with the behavior of the error of the non-linear fit applied over the magnetic measurements, for the computation of the calibration curves [10]. The maximum tune discrepancy goes up to -0.015 in the horizontal plane.

During LS2, the PSB was equipped with a B-train system which distributes the values from a real time B-field measurement, for the accurate measurement and control of the magnetic field in the dipoles. A new calibration curve was thus computed based on the B-train data and the measured excitation currents applied to the tune control. The results are shown in orange in Fig. 3. The tune difference in this case is smaller for R1 and similar in magnitude but opposite in sign for R2. The tune oscillations along the cycle are correlated with the error of the fit, as in the previous case. To avoid these oscillations, a Butterworth filter was applied for smoothing the B-train data and an interpolation between the

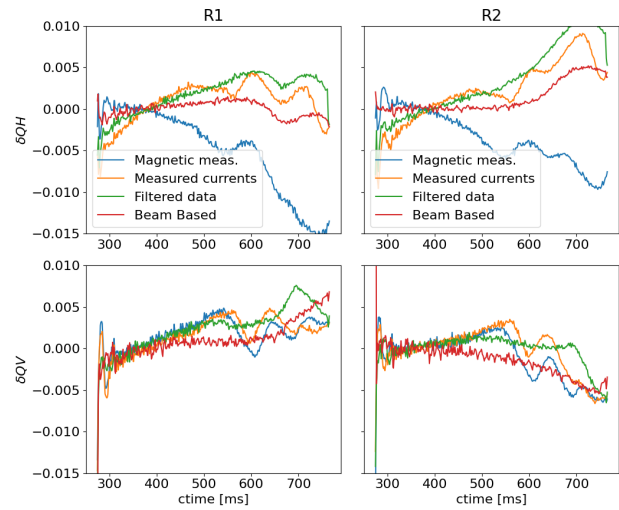


Figure 3: Difference between the set and measured tune as a function of the cycle time, for different calibration curves.

data points was used in the tune control application instead of the fit function. The impact of this calibration curve on the tunes is shown in green in Fig. 3. Indeed, by using the filtered data instead of a fit function, the tune oscillations along the cycle are eliminated.

The observed discrepancies between the set and measured tunes in all rings and in both planes indicate that the magnetic field actually seen by the beam is different both from the original magnetic measurements and the B-train measurements. One possible source that could explain these discrepancies is a time shift between the B-field and excitation current measurements, which can eventually explain an increased tune divergence along the cycle. In an attempt to correct these effects and flatten the tunes along the cycle, simultaneously for all rings, a beam based tune response approach was finally employed. In each time step, the  $\delta K_{f/d,i}$  which corresponds to the measured  $\delta Q$  is calculated, based on MAD-X [11] simulations. Assuming that this  $\delta K_{f/d,i}$  comes only from the calibration curve error, the correction over the smoothed calibration curve was computed based on Eq. (2). The results of these corrected calibration curves are shown in red in Fig. 3. This method led to a better flattening of the tune error for cycle times up to 600 ms. Although, an increase in the tune difference is observed after this time, the maximum discrepancy remains always below  $5 \times 10^{-3}$ . Investigations are ongoing for further simultaneous flattening of the tune error along the cycle, for all 4 rings and both planes.

## THE PS BOOSTER RE-ALIGNMENT CAMPAIGN

The PSB consists of four superposed rings, with the elements sharing the same physical support, as shown in Fig. 4. A tilt of one element would therefore lead to a different horizontal displacement (and thus closed orbit) of the beam for each ring.



Figure 4: The PSB quadrupole stack.

The basic optics cell of the PSB consists of: bending1-QF1-QD-QF2-bending2. Sixteen Beam Position Monitors (BPM) are available in the PSB for orbit measurements, with one BPM available per section which can measure in either plane (H or V). The pickups are installed in between the first focusing quadrupole (QF) and the defocusing quadrupole (QD).

### The PSB Alignment Tool

An alignment tool which takes into account simultaneously the four PSB rings has been developed. The tool follows a very similar approach to the one proposed for the orbit correction in the PSB in 2008 [12]. The minimization procedure is based on the ideal response matrix  $\vec{R}$ , which relates the orbit change at the BPMs ( $\Delta\vec{x}_0, \Delta\vec{y}_0$ ) with the horizontal and vertical displacements of the quadrupoles ( $\Delta\vec{x}, \Delta\vec{y}$ ):

$$\begin{pmatrix} \Delta\vec{x}_0 \\ \Delta\vec{y}_0 \end{pmatrix} = \vec{R} \cdot \begin{pmatrix} \Delta\vec{x} \\ \Delta\vec{y} \end{pmatrix}. \quad (4)$$

As the PSB quadrupoles share the same physical support for all four rings, the quadrupole displacements can not be separately assigned ring-by-ring. The elements of the vectors of the ring-by-ring displacements ( $\Delta\vec{x}_i, \Delta\vec{y}_i$ ) depend linearly on three sets of parameters: the horizontal and vertical displacements and the tilt angles of the quadrupole supports ( $\vec{\alpha}, \Delta\vec{x}, \Delta\vec{y}$ ). Assuming that R3 is the reference ring (the quadrupole supports can be tilted around R3) and with  $\Delta L$  being the vertical distance between two rings (0.36 m), the vector of the ring-by-ring displacements can be written as:

$$\begin{pmatrix} \Delta\vec{x}_1 \\ \Delta\vec{y}_1 \\ \Delta\vec{x}_2 \\ \Delta\vec{y}_2 \\ \Delta\vec{x}_3 \\ \Delta\vec{y}_3 \\ \Delta\vec{x}_4 \\ \Delta\vec{y}_4 \end{pmatrix} = \begin{pmatrix} -2\vec{I} & \vec{I} & \vec{0} \\ \vec{0} & \vec{0} & \vec{I} \\ -\vec{I} & \vec{I} & \vec{0} \\ \vec{0} & \vec{0} & \vec{I} \\ \vec{0} & \vec{I} & \vec{0} \\ \vec{0} & \vec{0} & \vec{I} \\ \vec{I} & \vec{I} & \vec{0} \\ \vec{0} & \vec{0} & \vec{I} \end{pmatrix} \cdot \begin{pmatrix} \Delta L \cdot \vec{\alpha} \\ \Delta x \\ \Delta y \end{pmatrix} = \vec{K} \cdot \begin{pmatrix} \Delta L \cdot \vec{\alpha} \\ \Delta x \\ \Delta y \end{pmatrix}, \quad (5)$$

where  $\vec{I}$  and  $\vec{0}$  the unitary and zero square matrices. Combining (4) and (5), the generalized inversion of the matrix  $\vec{R} \cdot \vec{K}$  is carried out using the Singular Value Decomposition

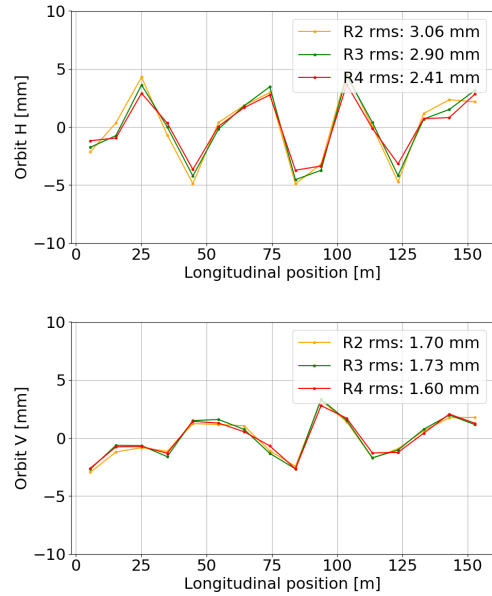


Figure 5: Measured orbits in R2, R3 and R4 in December 2020, before the machine re-alignment.

(SVD) technique and the vector of the required corrections will be given by:

$$\begin{pmatrix} \Delta L \cdot \vec{\alpha} \\ \Delta x \\ \Delta y \end{pmatrix} = -(\vec{R} \cdot \vec{K})^{-1} \cdot \begin{pmatrix} \Delta\vec{x}_{o1} \\ \Delta\vec{y}_{o1} \\ \Delta\vec{x}_{o2} \\ \Delta\vec{y}_{o2} \\ \Delta\vec{x}_{o3} \\ \Delta\vec{y}_{o3} \\ \Delta\vec{x}_{o4} \\ \Delta\vec{y}_{o4} \end{pmatrix} \quad (6)$$

The orbit correction calculation routine is based on the equations described above and was applied in a MICADO-like algorithm [13].

### Re-alignment Campaign after LS2

During LS2, the PSB went through major hardware changes. It was therefore decided to base the realignment proposal on a new orbit measurement campaign, during the PSB recommissioning period after LS2.

The new orbit measurement campaign was performed during the first days of the PSB beam recommissioning period, in December 2020. During this period, the BPM system was available only in R2, R3 and R4. Data were acquired for a flat 160 MeV cycle and a tune working point of  $(Q_H, Q_V) = (4.41, 4.23)$ . Figure 5 shows the rms orbit for R2, R3 and R4 in the horizontal (top) and vertical (bottom) planes. The orbit pattern is very similar to measurements performed in 2018, as expected since the upgrades applied during LS2 should not have an impact on the orbit.

To determine a set of efficient re-alignments for the simultaneous reduction of the bare orbits in all the four PSB

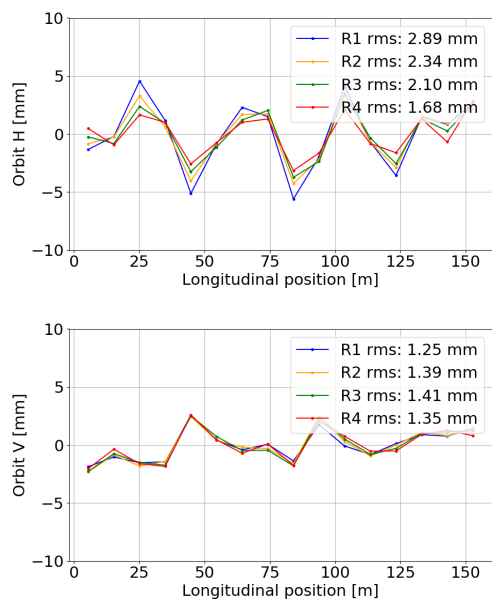


Figure 6: Measured orbits in R1, R2, R3 and R4 in February 2021, after the machine re-alignment.

rings, the horizontal and vertical displacement as well as roll angles of all quadrupoles were considered as potential correction knobs. A horizontal displacement of QDE7 by +1.12 mm and a vertical displacement of QDE13 by +0.19 mm were proposed and finally applied in the machine during the Christmas stop. The measured orbits after the re-alignment are presented in Fig. 6, for the horizontal (top) and vertical (bottom) planes, respectively. A reduction of the orbit was achieved in both planes, following nicely the tool predictions for all rings.

Even though the expected reduction of the orbit was achieved, an important ring-to-ring variation was still observed in the horizontal plane, pointing to possibly one or more roll angle misalignments in the machine.

As mentioned earlier, two special magnets are installed in the injection and extraction regions of each ring. The trim currents to compensate for differences with the main dipoles of the rings are computed based on the calibration curves from magnetic measurements. While for the initial orbit measurement campaign the correction functions for these special magnets were on, the uncertainty on the calibration curves from magnetic measurements led to the decision of switching off this correction for the bare orbit measurements.

The tool was then used to propose one or more re-alignment of elements that would minimize the ring-by-ring horizontal bare orbit differences. Based on this, a tilt of QFO31 by  $d\psi = 1.58$  mrad was proposed and finally applied in the machine during the Technical Stop of April 2021. Figure 7 shows the measured orbits before (top) and after (bottom) the alignment of QFO31 quadrupole. Indeed, this new alignment resulted in very similar orbits in all four rings, as predicted by the tool. The final minimization of the horizontal orbits was performed by using the trim circuits on the special injection and extraction magnets of each ring.

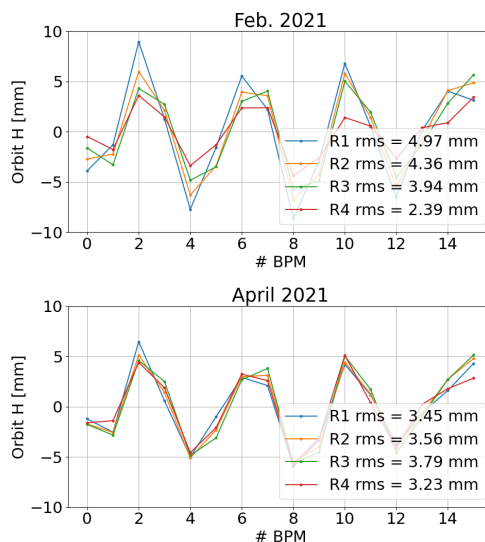


Figure 7: Orbit measurements before (top) and after (bottom) after the second machine re-alignment.

## CONCLUSION

The PS Booster came back into operation in December 2020, after a long shutdown period of two years, where major upgrades were applied to the machine. Two of the aspects leading to improved machine operation were discussed in this paper. A new tune control implementation, which takes into account the reconfiguration of the power supply circuits, the saturation of the main magnets and the increased complexity of the new  $H^-$  injection that was put in place during LS2 and commissioned during the recommissioning period. A successful implementation was demonstrated from the beginning, while a refinement of the calibration curves was required for full optimisation. Currently, the maximum difference between the set and measured tunes is of the order of  $5e-3$ . Further studies are ongoing to identify the source of this discrepancy. In the second part of the paper, the two re-alignment campaigns which took place in 2021 were presented. A minimization of the machine bare orbit was achieved, together with a minimization of the ring-to-ring orbit differences.

## ACKNOWLEDGEMENTS

The authors would like to thank the PSB Operations and commissioning teams for their support during the experiments. We would also like to thank A. Beaumont, A. Newborough and C. Petrone for all their input concerning the magnetic measurements.

## REFERENCES

- [1] J-M. Nonglaton and J-L. Sanchez Alvarez, "PSB Q-strips matrix reloaded", 2003, unpublished.
- [2] E. Renner *et al.*, "Beam Commissioning of the New 160 MeV  $H^-$  Injection System of the CERN PS Booster", in *Proc. 12th Int. Particle Accelerator Conf. (IPAC'21)*, Campinas,

- Brazil, May 2021, pp. 3116–3119. doi:10.18429/JACoW-IPAC2021-WEPAB210
- [3] A. Harle, “Power converters for quadrupole trim in the frameworks of the LIU-PSB project”, EDMS 1971638.
- [4] L. De Mallac, “Power converters for Qstrip magnets in the framework of the LIU-PSB project”, EDMS 1537264.
- [5] A. Parrella, J. Vella Wallbank, C. Petrone, R. Chritin, and M. Buzio, “Magnetic measurement results of the magnet PXMBHGC4WP-01000001 for the LIU-PSB project”, EDMS 2397540.
- [6] A. Parrella, J. Vella Wallbank, C. Petrone, R. Chritin, and M. Buzio, “Magnetic measurement results of the magnet PXMBHGC4WP-CR000003 for the LIU-PSB project”, EDMS 2213120.
- [7] A. Parrella, J. Vella Wallbank, C. Petrone, R. Chritin, and M. Buzio, “Magnetic measurement results of the magnet PXMBHGD4WP-CR000002 for the LIU-PSB project”, EDMS 2213024.
- [8] S. Albright, “PS Booster Magnetic Cycles to 1.4 and 2 GeV after LS2”, EDMS 1770413.
- [9] A. Parrella, J. Vella Wallbank, C. Petrone, R. Chritin, and M. Buzio, “Magnetic measurement results of the magnet PXMBHGC4WP-01000031 for the LIU-PSB project”, EDMS 2332909.
- [10] F. Antoniou *et al.*, “PSB beam commissioning: Orbits and tunes”, Presentation at ABP Injectors Working Group Meeting, CERN, Geneva, Switzerland, Mar. 2021. <https://indico.cern.ch/event/1013880/contributions/4255843/>
- [11] L. Deniau, E. Forest, H. Grote and F. Schmidt, computer code MAD-X, 2016. <http://madx.web.cern.ch/madx/>
- [12] M. Chanel, B. Mikulec, G. Rumolo, R. Tomas, “PS Booster Orbit Correction”, CERN-AB-2008-034 (ABP), unpublished.
- [13] B. Autin, Y. Marti, “Closed orbit correction of A.G.machines using a small number of magnets”, CERN, Geneva, Switzerland, CERN-ISR-MA-73-17, Mar. 1973.